
A DOUBLE-NORM AGGREGATED TENSOR LATENT FACTORIZATION MODEL FOR TEMPORAL-AWARE TRAFFIC SPEED IMPUTATION

Jiawen Hou

College of Computer and Information Science
Southwest University
Chongqing, China
h18761369818@email.swu.edu.cn

Hao Wu

College of Computer and Information Science
Southwest University
Chongqing, China
haowuf@gmail.com

ABSTRACT

In intelligent transportation systems (ITS), traffic management departments rely on sensors, cameras, and GPS devices to collect real-time traffic data. Traffic speed data is often incomplete due to sensor failures, data transmission delays, or occlusions, resulting in missing speed data in certain road segments. Currently, tensor decomposition based methods are extensively utilized, they mostly rely on the L_2 -norm to construct their learning objectives, which leads to reduced robustness in the algorithms. To address this, we propose Temporal-Aware Traffic Speed Imputation (TATSI), which combines the L_2 -norm and smooth L_1 (SL_1)-norm in its loss function, thereby achieving both high accuracy and robust performance in imputing missing time-varying traffic speed data. TATSI adopts a single latent factor-dependent, nonnegative, and multiplicative update (SLF-NMU) approach, which serves as an efficient solver for performing nonnegative latent factor analysis (LFA) on a tensor. Empirical studies on three real-world time-varying traffic speed datasets demonstrate that, compared with state-of-the-art traffic speed predictors, TATSI more precisely captures temporal patterns, thereby yielding the most accurate imputations for missing traffic speed data.

Keywords Intelligent Transportation Systems (ITS) · latent factorization of tensor · Traffic speed imputation · non-negativity constraint · smooth L_1 -norm · L_2 -norm

1 Introduction

With the continuous advancement of sensor and communication technologies, new traffic sensing devices have been widely deployed in ITS to collect massive spatio-temporal data [1], which would improve both the passenger experience and overall safety and efficiency [2]. These devices utilize advanced low-latency and highly reliable communication technologies including WiFi 6, low energy Bluetooth, and Ethernet to ensure that geographically [3] distributed sensors can transmit and share local sensing data effectively. Additionally, ITS [4] employ various machine learning (ML) methods to analyze the collected data, monitor the overall state of the road traffic network, and adaptively provide multiple functions [5] [6], such as congestion prevention and traffic flow optimization [7]. However, in practical applications, unpredictable factors such as network transmission interruptions, sensor failures [8], or storage device malfunctions often result in incomplete traffic data with numerous missing values [9]. Consequently, a significant portion of traffic speed data remains unobserved, and the extensive data volume collected over multiple days contributes to its incomplete nature [10]. Therefore, accurately and efficiently imputing unobserved traffic speed data remains a vital yet challenging issue [11].

Existing methods for missing value imputation typically rely on regression and probabilistic models [12], including techniques such as singular value decomposition [13], local least squares regression [14], probabilistic principal component analysis [15], Bayesian PCA [16], K-nearest neighbors [17], and missing forest imputation [18]. Despite their widespread use, these methods face several challenges [19]. For example, probabilistic models often assume specific data distributions, such as normality, which may not hold in practical scenarios [20]. Moreover, regression

models like local least squares tend to oversimplify complex, high-dimensional data [21], thereby limiting their performance [22].

Latent factorization of tensors (LFT)-based models have been extensively employed across various tensor analysis tasks. However, most existing LFT methods predominantly rely on the L_2 -norm [23], rendering them susceptible to outliers and significantly compromising their accuracy in data imputation tasks. In contrast, fewer methods utilize the L_1 -norm [24]. The L_1 -norm loss, in particular, demonstrates less sensitivity to large errors, thus enhancing the robustness of the models [25]. Moreover, it exhibits smoother behavior for small errors (i.e., errors with absolute values less than 1) [26], positively contributing to model stability [27]. Although LFT models employing L_2 -norm loss functions can generate stable predictions for missing data in high-dimensional tensor spaces [28], they generally lack robustness in the presence of outliers [29].

From the discussion above, it is evident that neither L_1 -norm nor L_2 -norm loss functions are optimal for modeling LFT models [30]. The SL_1 -norm loss is not only robust to large errors but also exhibits a smooth gradient when the absolute error is less than one [31]. Therefore, this study adopts a hybrid loss function that integrates both SL_1 -norm and L_2 -norm losses. In summary, this study makes two primary contributions:

1. A TATSI model, which efficiently combines the strong robustness of the SL_1 -norm loss with the stability of the L_2 -norm loss to accurately capture time-varying traffic speed data. Consequently, the model is robust to outliers in high-dimensional and incomplete (HDI) tensors and achieves high prediction accuracy for missing data.
2. We conduct experiments on three time-varying traffic speed datasets to evaluate the prediction accuracy and of our method.

The rest of the study is organized as follows: Section II describes the preliminaries, Section III proposes a TATSI method, Section IV depicts our experimental results in details, and section V concludes this article.

2 Preliminaries

2.1 Notations

In this study, we use a third-order traffic speed tensor constructed from observed speed measurements as the primary data source [32]. Since traffic speed data typically consists of non-negative real values, the resulting tensor is also non-negative, as illustrated in Fig. 1. Notably, the target tensor \mathbf{Y} usually exhibits high-dimensional incompleteness due to the presence of a large amount of unobserved data [33].

Definition 1 (Speed sensor-day-time tensor): Given the constructed tensor \mathbf{Y} , each element y_{ijk} denotes the observed traffic speed at sensor $i \in I$, on day $j \in J$, and at time $k \in K$, as shown in Fig. 1. Let Λ denote the set of observed elements and Γ denote the set of unobserved (unknown) elements.

2.2 Problem statement

In this study, we apply Canonical/Polyadic Tensor [26] to represent the tensor \mathbf{Y} into its latent factors [34]. Specifically, we express \mathbf{Y} as a sum of R rank-one tensors, $\mathbf{A}_1, \mathbf{A}_2, \dots, \mathbf{A}_R$, where R denotes the rank of the approximated tensor $\hat{\mathbf{Y}}$.

Definition 2: (Rank-One Tensor): A tensor $\mathbf{A}_r \in \mathbb{R}^{I \times J \times K}$ is a rank-one tensor which can be out produced by three latent factor (LF) vectors $\mathbf{s}_r, \mathbf{d}_r$, and \mathbf{t}_r as $\mathbf{A}_r = \mathbf{s}_r \circ \mathbf{d}_r \circ \mathbf{t}_r$ [35].

The LF matrices \mathbf{S}, \mathbf{D} , and \mathbf{T} consist of R latent factor vectors with dimensions $|I|, |J|$, and $|K|$, respectively, which are combined to form the r -th rank-one tensor \mathbf{A}_r [34]. The element-wise expression of \mathbf{A}_r is obtained by expanding the outer product of these three vectors [36].

$$a_{ijk} = s_{ir}d_{jr}t_{kr} \quad (1)$$

To obtain the desired latent factor (LF) matrices \mathbf{S}, \mathbf{D} , and \mathbf{T} , the Euclidean distance is typically employed as a similarity measure to quantify the difference between $\hat{\mathbf{Y}}$ and \mathbf{Y} within the LFT framework [20]. However, because only a few entries in \mathbf{Y} are observed, the objective function must be defined on the known dataset Λ to ensure accurate predictions [37]. Furthermore, non-negativity constraints are imposed on \mathbf{S}, \mathbf{D} , and \mathbf{T} to preserve their meaningful interpretation [38]. Therefore, the explicit objective function can be expressed as follows:

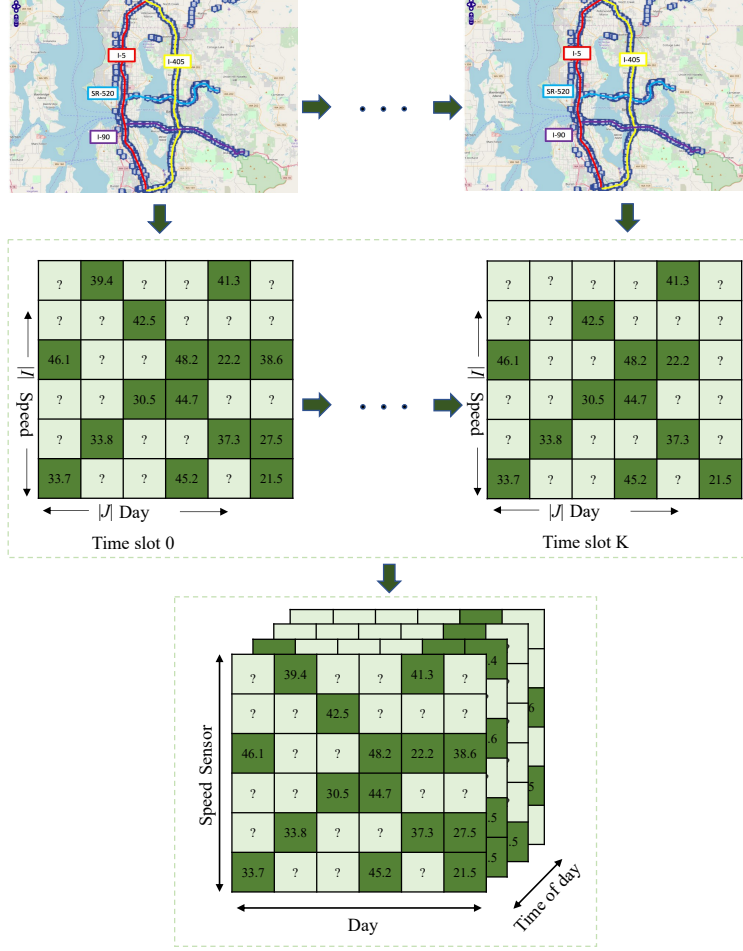


Figure 1: An example of the speed sensor-day-time tensor for traffic.

$$\begin{aligned}
\epsilon &= \sum_{y_{ijk} \in \Lambda} \left\| \mathbf{Y} - \hat{\mathbf{Y}} \right\|_F^2 = \sum_{y_{ijk} \in \Lambda} (y_{ijk} - \hat{y}_{ijk})^2 \\
&= \sum_{y_{ijk} \in \Lambda} \left(y_{ijk} - \sum_{r=1}^R s_{ir} d_{jr} t_{kr} \right)^2 \\
&\text{s.t. } \forall i \in I, \forall j \in J, \forall k \in K, r \in \{1, \dots, R\} : \\
&\quad s_{ir} \geq 0, d_{jr} \geq 0, t_{kr} \geq 0.
\end{aligned} \tag{2}$$

Definition 3: (SL_1 -norm of a Tensor): Given a tensor \mathbf{H} , symbol $\|\mathbf{H}\|_{SL_1}$ denotes the SL_1 -norm of \mathbf{H} .

$$\|\mathbf{H}\|_{SL_1} = \begin{cases} \sum_{l=1}^L \sum_{m=1}^M \sum_{n=1}^N h_{lmn}^2, & \text{if } |h_{lmn}| \leq 1, \\ \sum_{l=1}^L \sum_{m=1}^M \sum_{n=1}^N |h_{lmn}|, & \text{if } |h_{lmn}| > 1 \end{cases} \tag{3}$$

3 A TATSI method

3.1 Objective Function

To effectively characterize the latent structure of traffic speed tensors and improve prediction accuracy [39], loss functions based on the SL_1 -norm and L_2 -norm each offer distinct advantages for representing HDI data [40] [41]. Due to the known imbalance in the distribution of \mathbf{Y} and its sensitivity to the initial assumptions regarding S, D, and T [42], the problem is inherently ill-posed [43]. Consequently, it is essential to form a linear combination of the SL_1 -norm and the L_2 -norm to balance the model's generality and robustness [44]. To fully integrate these benefits, this paper proposes an objective function that combines the SL_1 -norm and L_2 -norm, as follows:

$$\begin{aligned} \varepsilon &= \|\Delta\|_{SL_1}^2 + \|\Delta\|_{L_2}^2 + \lambda (\|\mathbf{S}\|_F^2 + \|\mathbf{D}\|_F^2 + \|\mathbf{T}\|_F^2) \\ &= \sum_{y_{ijk} \in \Lambda} \left((\Delta_{ijk})_{SL_1}^2 + (\Delta_{ijk})_{L_2}^2 + \lambda \sum_{r=1}^R (s_{ir}^2 + d_{jr}^2 + t_{kr}^2) \right) \\ &\quad \text{s.t. } \forall i \in I, \forall j \in J, \forall k \in K, r \in \{1, \dots, R\} : \\ &\quad \quad s_{ir} \geq 0, d_{jr} \geq 0, t_{kr} \geq 0. \end{aligned} \quad (4)$$

The operator $\|\cdot\|_F$ computes the Frobenius norm between the observed and imputed values [45], thereby balancing the model's fit to the traffic speed data [46]. The norm $\|\cdot\|_{SL_1}$ represents the SL_1 -norm, which promotes sparsity in the factor matrices through a sparse regularization term [47], thereby suppressing noise and enhancing the model's robustness [48].

where Δ_{ijk} denotes the prediction error between y_{ijk} and \hat{y}_{ijk} , defined as:

$$\Delta_{ijk} = y_{ijk} - \hat{y}_{ijk} = y_{ijk} - \sum_{r=1}^R s_{ir} d_{jr} t_{kr}. \quad (5)$$

Here, \mathbf{Y} represents the observed traffic speed tensor containing missing values, while $\hat{\mathbf{Y}}$ denotes the reconstructed tensor obtained via decomposition [49] [50]. The factor matrices S, D, and T correspond, respectively, to speed sensors, days, and time of day [51].

Due to SL_1 -norm behaves differently when $|\Delta_{ijk}| \leq 1$ versus $|\Delta_{ijk}| > 1$, we rewrite the objective function (4) in a piecewise form to more accurately characterize the impact of errors on the model [52].

$$\begin{aligned} \varepsilon &= \begin{cases} \sum_{y_{ijk} \in \Lambda} \left(2(\Delta_{ijk})^2 + \lambda \sum_{r=1}^R (s_{ir}^2 + d_{jr}^2 + t_{kr}^2) \right), & \text{if } |\Delta_{ijk}| \leq 1, \\ \sum_{y_{ijk} \in \Lambda} \left(|\Delta_{ijk}| + (\Delta_{ijk})^2 + \lambda \sum_{r=1}^R (s_{ir}^2 + d_{jr}^2 + t_{kr}^2) \right), & \text{if } |\Delta_{ijk}| > 1, \end{cases} \\ &\quad \text{s.t. } \forall i \in I, \forall j \in J, \forall k \in K, \forall r \in \{1, \dots, R\} : \\ &\quad \quad s_{ir} \geq 0, d_{jr} \geq 0, t_{kr} \geq 0. \end{aligned} \quad (6)$$

3.2 Parameter Learning Procedure

Building upon the objective function discussed above, we introduce a single latent factor-dependent, nonnegative, and multiplicative update (SLF-NMU) strategy [53]. This method updates parameters via multiplicative adjustments at each iteration, thereby ensuring nonnegativity and accelerating convergence [54].

Within the gradient descent framework, the partial derivatives of ε with respect to s_{ir} , d_{jr} , and t_{kr} are computed [55] [56]. The general form of the gradient update can be expressed as follows:

$$(S, D, T) = \arg \min_{S, D, T} \varepsilon \Rightarrow \begin{cases} s_{ir} \leftarrow s_{ir} - \eta_{ir} \frac{\partial \varepsilon}{\partial s_{ir}} \\ d_{jr} \leftarrow d_{jr} - \eta_{jr} \frac{\partial \varepsilon}{\partial d_{jr}} \\ t_{kr} \leftarrow t_{kr} - \eta_{kr} \frac{\partial \varepsilon}{\partial t_{kr}} \end{cases} \quad (7)$$

Since the objective function employs a piecewise SL_1 -norm for Δ_{ijk} , the error is handled differently across various intervals [57]. Consequently, the corresponding gradient must also be computed in a piecewise manner. The partial derivative with respect to s_{ir} is shown in (8).

$$\frac{\partial \varepsilon}{\partial s_{ir}} = \begin{cases} \sum_{y_{ijk} \in \Lambda(i)} (d_{jr} t_{kr} - 2(y_{ijk} - \hat{y}_{ijk}) d_{jr} t_{kr} + 2\lambda s_{ir}), & \text{if } \Delta_{ijk} < -1, \\ \sum_{y_{ijk} \in \Lambda(i)} (-4(y_{ijk} - \hat{y}_{ijk}) d_{jr} t_{kr} + 2\lambda s_{ir}), & \text{if } |\Delta_{ijk}| \leq 1, \\ \sum_{y_{ijk} \in \Lambda(i)} (-d_{jr} t_{kr} - 2(y_{ijk} - \hat{y}_{ijk}) d_{jr} t_{kr} + 2\lambda s_{ir}), & \text{if } \Delta_{ijk} > 1. \end{cases} \quad (8)$$

Here, η_{ir} denotes the learning rate associated with the latent factor in the i -th dimension [58]. Due to the presence of negative terms in the formulation, latent factors may become negative during training [59]. To strictly enforce non-negativity, we adopt specific learning rate settings for each latent factor that eliminate negative values [60]. For simplicity, we present the derivation for S; similar derivations apply to D and T [61]. The updates are performed as follows:

$$\left\{ \begin{array}{l} \eta_{ir} = \frac{s_{ir}}{\sum_{y_{ijk} \in \Lambda(i)} (d_{jr} t_{kr} + 2\hat{y}_{ijk} d_{jr} t_{kr} + 2\lambda s_{ir})}, \quad \text{if } \Delta_{ijk} < -1, \\ \eta_{ir} = \frac{s_{ir}}{\sum_{y_{ijk} \in \Lambda(i)} (4\hat{y}_{ijk} d_{jr} t_{kr} + 2\lambda s_{ir})}, \quad \text{if } |\Delta_{ijk}| \leq 1, \\ \eta_{ir} = \frac{s_{ir}}{\sum_{y_{ijk} \in \Lambda(i)} (2\hat{y}_{ijk} d_{jr} t_{kr} + 2\lambda s_{ir})}, \quad \text{if } \Delta_{ijk} > 1. \end{array} \right. \quad (9)$$

Substituting (8) and (9) into (7) and simplifying, we obtain the following update rule (10):

$$s_{ir} \leftarrow \begin{cases} s_{ir} \frac{\sum_{y_{ijk} \in \Lambda(i)} 2y_{ijk} d_{jr} t_{kr}}{\sum_{y_{ijk} \in \Lambda(i)} (d_{jr} t_{kr} + 2\hat{y}_{ijk} d_{jr} t_{kr} + 2\lambda s_{ir})}, & \text{if } \Delta_{ijk} < -1, \\ s_{ir} \frac{\sum_{y_{ijk} \in \Lambda(i)} 4y_{ijk} d_{jr} t_{kr}}{\sum_{y_{ijk} \in \Lambda(i)} (4\hat{y}_{ijk} d_{jr} t_{kr} + 2\lambda s_{ir})}, & \text{if } |\Delta_{ijk}| \leq 1, \\ s_{ir} \frac{\sum_{y_{ijk} \in \Lambda(i)} (d_{jr} t_{kr} + 2y_{ijk} d_{jr} t_{kr})}{\sum_{y_{ijk} \in \Lambda(i)} (2\hat{y}_{ijk} d_{jr} t_{kr} + 2\lambda s_{ir})}, & \text{if } \Delta_{ijk} > 1. \end{cases} \quad (10)$$

4 Empirical studies

4.1 Experimental Setup

Datasets: This study employs three publicly available traffic speed datasets. D1 was collected by inductive loop detectors deployed on highways in the Seattle area, USA [62]. A total of 323 loop detectors were selected, recording traffic speeds every 5 minutes, resulting in 288 measurements per sensor per day [63]. Thus, the traffic data is organized as tensor $\mathbf{A}^{(1)} \in \mathbb{R}^{323 \times 288 \times 288}$. D2 comprises traffic speed data collected from 214 anonymous road segments (mainly urban expressways and arterial roads) in Guangzhou [64], China, over two months (61 days, from August 1 to September 30, 2016), with intervals of 10 minutes. Thus, the traffic data is organized as tensor $\mathbf{A}^{(2)} \in \mathbb{R}^{214 \times 61 \times 144}$. D3 consists of traffic speed data collected in urban areas with 18 road segments over 28 days, with a sampling interval of 5 minutes (resulting in 288 time windows per day). Thus, this traffic data is organized as tensor $\mathbf{A}^{(3)} \in \mathbb{R}^{18 \times 28 \times 288}$. In order to ensure a robust evaluation of the proposed model and to mitigate overfitting, each dataset is partitioned in two ways for training, validation, and testing: 10%:20%:70% and 20%:20%:60%, respectively, which are shown in TABLE 1.

Table 1: Datasets

Datasets		$ \Omega : \Psi : \Phi $	Total Entries	Sensor Count	Day Count	Time Count
D1	D1.1	10%:20%:70%	92,885	323	28	288
	D1.2	20%:20%:60%	92,885	323	28	288
D2	D2.1	10%:20%:70%	49,925	214	61	144
	D2.2	20%:20%:60%	49,925	214	61	144
D3	D3.1	10%:20%:70%	92,885	18	28	288
	D3.2	20%:20%:60%	92,885	18	28	288

Evaluation Metrics: We emphasize the accuracy of traffic speed imputations, as it directly indicates whether the model has captured the essential characteristics of an HDI tensor [65]. Consequently, we employ the mean absolute error (MAE) and root mean square error (RMSE) as evaluation metrics. Let \hat{y}_{ijk} and y_{ijk} denote the estimated and actual values, respectively [8]. The two expressions are defined as follows [66]:

$$\begin{aligned}
 \text{RMSE} &= \sqrt{\frac{1}{|\Phi|} \sum_{y_{ijk} \in \Phi} (y_{ijk} - \hat{y}_{ijk})^2} \\
 \text{MAE} &= \frac{1}{|\Phi|} \sum_{y_{ijk} \in \Phi} |y_{ijk} - \hat{y}_{ijk}|
 \end{aligned} \tag{11}$$

For a tested model, small RMSE and MAE value express high prediction accuracy.

Experiment Details: To ensure a fair evaluation of model performance, all models were implemented on an i7 CPU in a Java (JDK 1.8) environment. Convergence is determined when the loss difference between two consecutive iterations falls below 10^{-5} or when the number of iterations exceeds 1000.

Baselines: To evaluate the performance of the proposed TATSI, we compare it against the following state-of-the-art models: *M2* (a quality-of-service prediction model employing the classic Frobenius loss without bias [67]), *M3* (an integrated environment QoS prediction model [68]), and *M4* (a QoS prediction model utilizing the Cauchy loss [69]). To ensure a fair comparison, the latent feature dimension R for all models is set to 20.

Hyperparameter Settings: The hyperparameter that affects the performance of mine model is the regularization coefficient λ . We search λ from the range $[2^{-20}, 2^0]$ with a step size of 2^{-1} , and finally decide to set $\lambda = 9.765625 \times 10^{-4}$ on *D1* and *D2*, and set $\lambda = 1.0$ on *D3*. For the hyperparameters of other baselines, they are fine-tuned from the settings in their papers.

4.2 Experimental Results and Analysis

Table II records the RMSE and MAE of M1–M4 on four cases. Fig. 2 and Fig. 3 show the RMSE and MAE of all models. From the results, we conduct the following analysis:

Table 2: RMSE and MAE of M1-M4 on datasets

Datasets		M1	M2	M3	M4
D1.1	RMSE	5.5488	5.6154	5.8454	5.5947
	MAE	3.4083	3.4829	3.6865	3.4694
D1.2	RMSE	5.4963	5.5039	5.5322	5.5008
	MAE	3.3782	3.4132	3.4624	3.3980
D2.1	RMSE	4.2949	4.3139	4.6317	4.3179
	MAE	2.8414	2.8799	3.1242	2.8765
D2.2	RMSE	4.2476	4.3356	4.3540	4.2378
	MAE	2.7841	2.8052	2.9043	2.7967
D3.1	RMSE	9.9916	10.2205	10.8299	10.4492
	MAE	7.0067	7.2274	7.7656	7.3937
D3.2	RMSE	8.9619	9.1044	9.6073	9.0432
	MAE	6.2427	6.3014	6.8097	6.2948

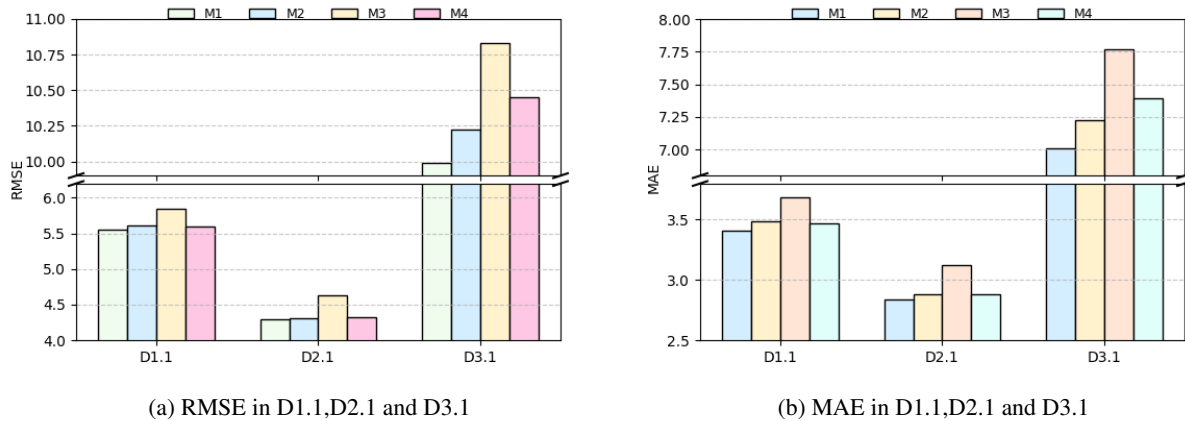


Figure 2: RMSE and MAE on the 10% training set

(a) The RMSE and MAE achieved by TATSI are lower than those of the other three models on datasets D1.1, D2.1, and D3.1. As shown in Table 2 and Fig. 2, the minimum RMSE achieved by M1 on D1.1 is 5.5488, which is 1.19% lower than M2’s (5.6154), 5.07% lower than M3’s (5.8454), and 0.82% lower than M4’s (5.5947), respectively. Similarly, the minimum MAE achieved by M1 on D1.1 is 3.4083, which is 2.14% lower than M2’s (3.4829), 7.55% lower than M3’s (3.6865), and 1.76% lower than M4’s (3.4694). On D2.1, the minimum RMSE achieved by M1 is 4.2949, representing a 0.44% reduction relative to M2’s (4.3139), a 7.27% reduction relative to M3’s (4.6317), and a 0.53% reduction relative to M4’s (4.3179). Additionally, the minimum MAE achieved by M1 on D2.1 is 2.8414, which is 1.34% lower than M2’s (2.8799), 9.05% lower than M3’s (3.1242), and 1.22% lower than M4’s (2.8765). For D3.1, the minimum RMSE achieved by M1 is 9.9916, corresponding to a 2.24% decrease compared to M2’s (10.2205), a 7.74% decrease compared to M3’s (10.8299), and a 4.38% decrease compared to M4’s (10.4492). Similarly, the minimum MAE achieved by M1 on D3.1 is 7.0067, which is 3.05% lower than M2’s (7.2274), 9.78% lower than M3’s (7.7656), and 5.23% lower than M4’s (7.3937), respectively. These results demonstrate that TATSI achieves superior traffic speed prediction accuracy. A similar conclusion can be drawn from the other cases shown in Fig. 3.

(b) As the proportion of training data increases, the TATSI model still demonstrates superior imputation accuracy. Specifically, for dataset D1.2, the minimum RMSE achieved by M1 is 5.4963, which is 0.14% lower than M2’s 5.5039,

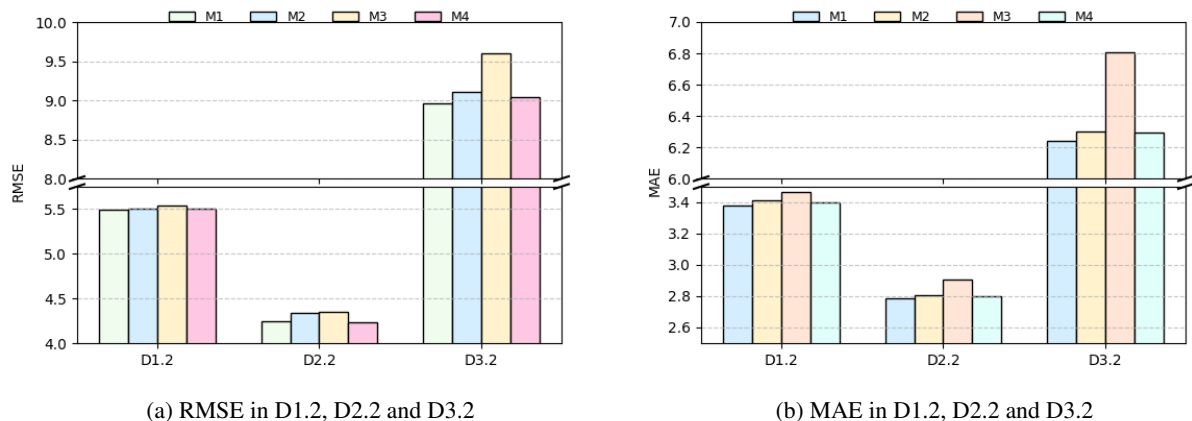


Figure 3: RMSE and MAE on the 20% training set

0.65% lower than M3’s 5.5322, and 0.08% lower than M4’s 5.5008. Similarly, the minimum MAE achieved by M1 on D1.2 is 3.3782, which is 1.03% lower than M2’s 3.4132, 2.43% lower than M3’s 3.4624, and 0.58% lower than M4’s 3.3980. For dataset D2.2, the minimum RMSE achieved by M1 is 4.2476, representing a 2.03% reduction compared to M2’s 4.3356 and a 2.44% reduction compared to M3’s 4.3540, although it is 0.23% higher than M4’s 4.2378. In terms of MAE, M1 attains a minimum value of 2.7841 on D2.2, which is 0.75% lower than M2’s 2.8052, 4.14% lower than M3’s 2.9043, and 0.45% lower than M4’s 2.7967. For dataset D3.2, the minimum RMSE achieved by M1 is 8.9619, which is 1.57% lower than M2’s 9.1044, 6.72% lower than M3’s 9.6073, and 0.90% lower than M4’s 9.0432. Moreover, the minimum MAE achieved by M1 on D3.2 is 6.2427, which is 0.93% lower than M2’s 6.3014, 8.33% lower than M3’s 6.8097, and 0.83% lower than M4’s 6.2948.

5 Conclusion

To accurately impute unobserved time-varying traffic speed data, this study proposes the Temporal-Aware Traffic Speed Imputation (TATSI) model. The model employs a combination of the SL_1 -norm and L_2 -norm in its loss function, along with robust regularization, which together confer both robustness and high accuracy in imputing missing data from an HDI tensor. Experimental results on three real-world time-varying traffic speed datasets demonstrate that TATSI significantly outperforms state-of-the-art models in prediction accuracy for missing data from an HDI tensor. Furthermore, developing an adaptive strategy for the hyperparameter λ presents an interesting challenge, which we plan to investigate in future work.

References

- [1] X. Luo, Y. Yuan, S. Chen, N. Zeng, and Z. Wang, “Position-transitional particle swarm optimization-incorporated latent factor analysis,” *IEEE Transactions on Knowledge and Data Engineering*, vol. 34, no. 8, pp. 3958–3970, 2020.
- [2] O. Avatefipour and F. Sadry, “Traffic management system using iot technology-a comparative review,” in *2018 IEEE International Conference on Electro/Information Technology (EIT)*. IEEE, 2018, pp. 1041–1047.
- [3] A. Pascale, M. Nicoli, F. Deflorio, B. Dalla Chiara, and U. Spagnolini, “Wireless sensor networks for traffic management and road safety,” *IET Intelligent Transport Systems*, vol. 6, no. 1, pp. 67–77, 2012.
- [4] L. Zhu, F. R. Yu, Y. Wang, B. Ning, and T. Tang, “Big data analytics in intelligent transportation systems: A survey,” *IEEE Transactions on Intelligent Transportation Systems*, vol. 20, no. 1, pp. 383–398, 2018.
- [5] D. Wu, X. Luo, M. Shang, Y. He, G. Wang, and X. Wu, “A data-characteristic-aware latent factor model for web services qos prediction,” *IEEE Transactions on Knowledge and Data Engineering*, vol. 34, no. 6, pp. 2525–2538, 2020.
- [6] W. Yang, S. Li, Z. Li, and X. Luo, “Highly accurate manipulator calibration via extended kalman filter-incorporated residual neural network,” *IEEE Transactions on Industrial Informatics*, vol. 19, no. 11, pp. 10 831–10 841, 2023.

- [7] P. Tang, T. Ruan, H. Wu, and X. Luo, “Temporal pattern-aware qos prediction by biased non-negative tucker factorization of tensors,” *Neurocomputing*, vol. 582, p. 127447, 2024.
- [8] X. Luo, Y. Zhou, Z. Liu, and M. Zhou, “Fast and accurate non-negative latent factor analysis of high-dimensional and sparse matrices in recommender systems,” *IEEE Transactions on Knowledge and Data Engineering*, vol. 35, no. 4, pp. 3897–3911, 2021.
- [9] P. Wang, T. Hu, F. Gao, R. Wu, W. Guo, and X. Zhu, “A hybrid data-driven framework for spatiotemporal traffic flow data imputation,” *IEEE Internet of Things Journal*, vol. 9, no. 17, pp. 16 343–16 352, 2022.
- [10] D. Wu, P. Zhang, Y. He, and X. Luo, “A double-space and double-norm ensembled latent factor model for highly accurate web service qos prediction,” *IEEE Transactions on Services Computing*, vol. 16, no. 2, pp. 802–814, 2022.
- [11] D. Wu, X. Luo, Y. He, and M. Zhou, “A prediction-sampling-based multilayer-structured latent factor model for accurate representation to high-dimensional and sparse data,” *IEEE transactions on neural networks and learning systems*, vol. 35, no. 3, pp. 3845–3858, 2022.
- [12] Q. Li, H. Tan, Y. Wu, L. Ye, and F. Ding, “Traffic flow prediction with missing data imputed by tensor completion methods,” *IEEE Access*, vol. 8, pp. 63 188–63 201, 2020.
- [13] Y. Liu, T. Dillon, W. Yu, W. Rahayu, and F. Mostafa, “Missing value imputation for industrial iot sensor data with large gaps,” *IEEE Internet of Things Journal*, vol. 7, no. 8, pp. 6855–6867, 2020.
- [14] H. Kim, G. H. Golub, and H. Park, “Missing value estimation for dna microarray gene expression data: local least squares imputation,” *Bioinformatics*, vol. 21, no. 2, pp. 187–198, 2005.
- [15] M. E. Tipping and C. M. Bishop, “Probabilistic principal component analysis,” *Journal of the Royal Statistical Society Series B: Statistical Methodology*, vol. 61, no. 3, pp. 611–622, 1999.
- [16] H. Li, Y. Wang, and M. Li, “A bpca based missing value imputation and its impact on traffic incident prediction,” in *18th COTA International Conference of Transportation Professionals*. American Society of Civil Engineers Reston, VA, 2018, pp. 1782–1791.
- [17] G. E. Batista and M. C. Monard, “An analysis of four missing data treatment methods for supervised learning,” *Applied artificial intelligence*, vol. 17, no. 5-6, pp. 519–533, 2003.
- [18] D. J. Stekhoven and P. Bühlmann, “Missforest—non-parametric missing value imputation for mixed-type data,” *Bioinformatics*, vol. 28, no. 1, pp. 112–118, 2012.
- [19] H. Wu, Y. Qiao, and X. Luo, “A fine-grained regularization scheme for non-negative latent factorization of high-dimensional and incomplete tensors,” *IEEE Transactions on Services Computing*, vol. 17, no. 6, pp. 3006–3021, 2024.
- [20] H. Wu, X. Luo, and M. Zhou, “Advancing non-negative latent factorization of tensors with diversified regularization schemes,” *IEEE Transactions on Services Computing*, vol. 15, no. 3, pp. 1334–1344, 2020.
- [21] L. Hu, S. Yang, X. Luo, and M. Zhou, “An algorithm of inductively identifying clusters from attributed graphs,” *IEEE Transactions on Big Data*, vol. 8, no. 2, pp. 523–534, 2020.
- [22] X. Luo, H. Wu, Z. Wang, J. Wang, and D. Meng, “A novel approach to large-scale dynamically weighted directed network representation,” *IEEE Transactions on Pattern Analysis and Machine Intelligence*, vol. 44, no. 12, pp. 9756–9773, 2021.
- [23] Z. Liu, X. Luo, and Z. Wang, “Convergence analysis of single latent factor-dependent, nonnegative, and multiplicative update-based nonnegative latent factor models,” *IEEE Transactions on Neural Networks and Learning Systems*, vol. 32, no. 4, pp. 1737–1749, 2020.
- [24] X. Luo, M. Zhou, S. Li, Z. You, Y. Xia, and Q. Zhu, “A nonnegative latent factor model for large-scale sparse matrices in recommender systems via alternating direction method,” *IEEE transactions on neural networks and learning systems*, vol. 27, no. 3, pp. 579–592, 2015.
- [25] C. Leng, H. Zhang, G. Cai, I. Cheng, and A. Basu, “Graph regularized lp smooth non-negative matrix factorization for data representation,” *IEEE/CAA Journal of Automatica Sinica*, vol. 6, no. 2, pp. 584–595, 2019.
- [26] L. Hu, J. Zhang, X. Pan, X. Luo, and H. Yuan, “An effective link-based clustering algorithm for detecting overlapping protein complexes in protein-protein interaction networks,” *IEEE Transactions on Network Science and Engineering*, vol. 8, no. 4, pp. 3275–3289, 2021.
- [27] Y. Yuan, X. Luo, M. Shang, and Z. Wang, “A kalman-filter-incorporated latent factor analysis model for temporally dynamic sparse data,” *IEEE Transactions on Cybernetics*, vol. 53, no. 9, pp. 5788–5801, 2022.

- [28] Y. Koren, S. Rendle, and R. Bell, “Advances in collaborative filtering,” *Recommender systems handbook*, pp. 91–142, 2021.
- [29] X. Luo, H. Wu, and Z. Li, “Neulft: A novel approach to nonlinear canonical polyadic decomposition on high-dimensional incomplete tensors,” *IEEE Transactions on Knowledge and Data Engineering*, vol. 35, no. 6, pp. 6148–6166, 2022.
- [30] H. Wu and X. Luo, “Instance-frequency-weighted regularized, nonnegative and adaptive latent factorization of tensors for dynamic qos analysis,” in *2021 IEEE International Conference on Web Services (ICWS)*. IEEE, 2021, pp. 560–568.
- [31] X. Luo, Y. Zhong, Z. Wang, and M. Li, “An alternating-direction-method of multipliers-incorporated approach to symmetric non-negative latent factor analysis,” *IEEE Transactions on Neural Networks and Learning Systems*, vol. 34, no. 8, pp. 4826–4840, 2021.
- [32] W. Li, X. Luo, H. Yuan, and M. Zhou, “A momentum-accelerated hessian-vector-based latent factor analysis model,” *IEEE Transactions on Services Computing*, vol. 16, no. 2, pp. 830–844, 2022.
- [33] H. Wu, X. Wu, and X. Luo, *Dynamic Network Representation Based on Latent Factorization of Tensors*. Springer, 2023.
- [34] H. Wu, X. Luo, M. Zhou, M. J. Rawa, K. Sedraoui, and A. Albeshri, “A pid-incorporated latent factorization of tensors approach to dynamically weighted directed network analysis,” *IEEE/CAA Journal of Automatica Sinica*, vol. 9, no. 3, pp. 533–546, 2021.
- [35] X. Luo, Z. Li, W. Yue, and S. Li, “A calibrator fuzzy ensemble for highly-accurate robot arm calibration,” *IEEE Transactions on Neural Networks and Learning Systems*, 2024.
- [36] F. Bi, T. He, Y. Xie, and X. Luo, “Two-stream graph convolutional network-incorporated latent feature analysis,” *IEEE Transactions on Services Computing*, vol. 16, no. 4, pp. 3027–3042, 2023.
- [37] Y. Yuan, J. Li, and X. Luo, “A fuzzy pid-incorporated stochastic gradient descent algorithm for fast and accurate latent factor analysis,” *IEEE Transactions on Fuzzy Systems*, 2024.
- [38] H. Wu, X. Luo, and M. Zhou, “Discovering hidden pattern in large-scale dynamically weighted directed network via latent factorization of tensors,” in *2021 IEEE 17th International Conference on Automation Science and Engineering (CASE)*. IEEE, 2021, pp. 1533–1538.
- [39] W. Yang, S. Li, and X. Luo, “Data driven vibration control: A review,” *IEEE/CAA Journal of Automatica Sinica*, vol. 11, no. 9, pp. 1898–1917, 2024.
- [40] T. Goldstein and S. Osher, “The split bregman method for l_1 -regularized problems,” *SIAM journal on imaging sciences*, vol. 2, no. 2, pp. 323–343, 2009.
- [41] D. Wu, Y. He, and X. Luo, “A graph-incorporated latent factor analysis model for high-dimensional and sparse data,” *IEEE transactions on emerging topics in computing*, vol. 11, no. 4, pp. 907–917, 2023.
- [42] X. Liao, K. Hoang, and X. Luo, “Local search-based anytime algorithms for continuous distributed constraint optimization problems,” *IEEE/CAA Journal of Automatica Sinica*, vol. 12, no. 1, pp. 288–290, 2025.
- [43] A. Zeng and H. Wu, “A fast and inherently nonnegative latent factorization of tensors model for dynamic directed network representation,” in *2024 27th International Conference on Computer Supported Cooperative Work in Design (CSCWD)*. IEEE, 2024, pp. 2955–2960.
- [44] H. Wu, Y. Xia, and X. Luo, “Proportional-integral-derivative-incorporated latent factorization of tensors for large-scale dynamic network analysis,” in *2021 China Automation Congress (CAC)*. IEEE, 2021, pp. 2980–2984.
- [45] Y. Zhong, K. Liu, S. Gao, and X. Luo, “Alternating-direction-method of multipliers-based adaptive nonnegative latent factor analysis,” *IEEE Transactions on Emerging Topics in Computational Intelligence*, 2024.
- [46] M. Chen and H. Wu, “Efficient representation to dynamic qos data via momentum-incorporated biased nonnegative and adaptive latent factorization of tensors,” in *2021 International Conference on Cyber-Physical Social Intelligence (ICCSI)*. IEEE, 2021, pp. 1–6.
- [47] J. Chen, Y. Yuan, and X. Luo, “Sdgnn: Symmetry-preserving dual-stream graph neural networks,” *IEEE/CAA journal of automatica sinica*, vol. 11, no. 7, pp. 1717–1719, 2024.
- [48] X. Luo, M. Chen, H. Wu, Z. Liu, H. Yuan, and M. Zhou, “Adjusting learning depth in nonnegative latent factorization of tensors for accurately modeling temporal patterns in dynamic qos data,” *IEEE Transactions on Automation Science and Engineering*, vol. 18, no. 4, pp. 2142–2155, 2021.
- [49] J. Wang, W. Li, and X. Luo, “A distributed adaptive second-order latent factor analysis model,” *IEEE/CAA Journal of Automatica Sinica*, 2024.

- [50] L. Hu, Y. Yang, Z. Tang, Y. He, and X. Luo, "Fcan-mopso: an improved fuzzy-based graph clustering algorithm for complex networks with multiobjective particle swarm optimization," *IEEE Transactions on Fuzzy Systems*, vol. 31, no. 10, pp. 3470–3484, 2023.
- [51] Q. Jiang, D. Liu, H. Zhu, S. Wu, N. Wu, X. Luo, and Y. Qiao, "Iterative role negotiation via the bilevel gra++ with decision tolerance," *IEEE Transactions on Computational Social Systems*, 2024.
- [52] W. Qin and X. Luo, "Asynchronous parallel fuzzy stochastic gradient descent for high-dimensional incomplete data representation," *IEEE Transactions on Fuzzy Systems*, vol. 32, no. 2, pp. 445–459, 2023.
- [53] X. Luo, M. Zhou, Y. Xia, and Q. Zhu, "An efficient non-negative matrix-factorization-based approach to collaborative filtering for recommender systems," *IEEE Transactions on Industrial Informatics*, vol. 10, no. 2, pp. 1273–1284, 2014.
- [54] H. Fang, Q. Wang, Q. Hu, and H. Wu, "Modularity maximization-incorporated nonnegative tensor rescal decomposition for dynamic community detection," in *2024 IEEE International Conference on Systems, Man, and Cybernetics (SMC)*. IEEE, 2024, pp. 1871–1876.
- [55] W. Qin, X. Luo, and M. Zhou, "Adaptively-accelerated parallel stochastic gradient descent for high-dimensional and incomplete data representation learning," *IEEE Transactions on Big Data*, vol. 10, no. 1, pp. 92–107, 2023.
- [56] F. Bi, X. Luo, B. Shen, H. Dong, and Z. Wang, "Proximal alternating-direction-method-of-multipliers-incorporated nonnegative latent factor analysis," *IEEE/CAA Journal of Automatica Sinica*, vol. 10, no. 6, pp. 1388–1406, 2023.
- [57] T. Chen, S. Li, Y. Qiao, and X. Luo, "A robust and efficient ensemble of diversified evolutionary computing algorithms for accurate robot calibration," *IEEE Transactions on Instrumentation and Measurement*, vol. 73, pp. 1–14, 2024.
- [58] G. Liu and H. Wu, "Hp-csf: An gpu optimization method for cp decomposition of incomplete tensors," in *IFIP International Conference on Network and Parallel Computing*. Springer, 2024, pp. 77–90.
- [59] N. Zeng, X. Li, P. Wu, H. Li, and X. Luo, "A novel tensor decomposition-based efficient detector for low-altitude aerial objects with knowledge distillation scheme," *IEEE/CAA Journal of Automatica Sinica*, vol. 11, no. 2, pp. 487–501, 2024.
- [60] Q. Wang and H. Wu, "Dynamically weighted directed network link prediction using tensor ring decomposition," in *2024 27th International Conference on Computer Supported Cooperative Work in Design (CSCWD)*. IEEE, 2024, pp. 2864–2869.
- [61] J. Li, F. Tan, C. He, Z. Wang, H. Song, P. Hu, and X. Luo, "Saliency-aware dual embedded attention network for multivariate time-series forecasting in information technology operations," *IEEE Transactions on Industrial Informatics*, vol. 20, no. 3, pp. 4206–4217, 2023.
- [62] Z. Cui, R. Ke, and Y. Wang, "Deep bidirectional and unidirectional lstm recurrent neural network for network-wide traffic speed prediction," *arXiv preprint arXiv:1801.02143*, 2018.
- [63] Z. Cui, K. Henrickson, R. Ke, and Y. Wang, "Traffic graph convolutional recurrent neural network: A deep learning framework for network-scale traffic learning and forecasting," *IEEE Transactions on Intelligent Transportation Systems*, 2019.
- [64] X. Chen, Z. He, and J. Wang, "Spatial-temporal traffic speed patterns discovery and incomplete data recovery via svd-combined tensor decomposition," *Transportation research part C: emerging technologies*, vol. 86, pp. 59–77, 2018.
- [65] H. Wu, X. Luo, and M. Zhou, "Neural latent factorization of tensors for dynamically weighted directed networks analysis," in *2021 IEEE International Conference on Systems, Man, and Cybernetics (SMC)*. IEEE, 2021, pp. 3061–3066.
- [66] X. Luo, L. Wang, P. Hu, and L. Hu, "Predicting protein-protein interactions using sequence and network information via variational graph autoencoder," *IEEE/ACM Transactions on Computational Biology and Bioinformatics*, vol. 20, no. 5, pp. 3182–3194, 2023.
- [67] X. Luo, H. Wu, H. Yuan, and M. Zhou, "Temporal pattern-aware qos prediction via biased non-negative latent factorization of tensors," *IEEE transactions on cybernetics*, vol. 50, no. 5, pp. 1798–1809, 2019.
- [68] X. Su, M. Zhang, Y. Liang, Z. Cai, L. Guo, and Z. Ding, "A tensor-based approach for the qos evaluation in service-oriented environments," *IEEE Transactions on Network and Service Management*, vol. 18, no. 3, pp. 3843–3857, 2021.
- [69] F. Ye, Z. Lin, C. Chen, Z. Zheng, and H. Huang, "Outlier-resilient web service qos prediction," in *Proceedings of the web conference 2021*, 2021, pp. 3099–3110.